유한요소·경계요소병용법을 이용한 전기자동차용 동기전동기의 개발 및 성능향상에 관한 연구

論 文
49B - 3 - 5

Development of the Synchronous Motors for Electric Vehicle and Improvement of the Performance by Hybrid Finite Element and Boundary Element Method

田 宇 鎭* · 渡 辺 英 樹** · 紙 屋 雄 史*** · 小 貫 天§ · 田 惠 晶§§
(Woojin Jeon · Hideki Watanabe · Yushi Kamiya · Takashi Onuki · Hyejeong Jeon)

Abstract - This paper treats the optimization of rotor construction in the permanent magnet synchronous motor (PMSM) for electric vehicle (EV). While the field system of PMSM has generally one magnet per pole, we replace the magnet into plural sub-magnets. The dimensions of each sub-magnet are determined by the concept of pulse width modulation (PWM). By adopting the proposed rotor construction, we can not only reduce the space harmonics of the air-gap field but also provide space for rotor bars (i.e., damper windings) around the direct-axis. From the investigation by hybrid FE-BE (coupled finite element and boundary element) method coupled with both electric circuit and motion equation, we verify that the proposed construction is effective for practical use.

Key Words : PMSM, EV, PWM, Space harmonics, Damper winding, Hybrid FE-BE method

1. Introduction

While the field system of PMSM for EV has generally a single magnet for a main-pole, we adopt plural magnets having the same polarity. The plural magnets are referred to as a sub-magnets hereafter. By using this sub-magnet scheme, we can reduce undesirable higher space harmonics in electric machinery. To obtain the dimensions and arrangements of sub-magnets, we quote our own method based on the concept of PWM. In addition, by using such a sub-magnet scheme, the space for damper windings is provided between neighboring sub-ones.

We first investigate the validity of the proposed rotor construction from the standpoint of both the space harmonic reduction and the damping effects by two dimensional (2-D) hybrid FE-BE method. To obtain the dynamic and transient characteristics, we couple the method with both electric circuit and motion equation. Then, we confirm by experiments that the proposed motor is suitable for electric vehicle (EV) in view of the followings : the ratio of space harmonics to the fundamental component, hunting oscillations, self-starting, and the feasibility of manufacture.

* 正 會 員 : 日本 早稻田大 理工學部 敎員 · 工博
** 非 會 員 : (株) SONY 社員
*** 非 會 員 : 日本 國立群馬大 敎育學硏究科 助敎授 · 工博
§ 非 會 員 : 日本 早稻田大 理工學部 敎授 · 工博
§§ 非 會 員 : LG綜合技術院 先任硏究員
韓國科學技術院 電算學科 博士課程
接受日字 : 1999年 9月 2日
最終完了 : 2000年 1月 5日

2. Principle & Structure

Assuming that the flux density developed by permanent magnet made of rear-earth one distributes rectangularly, the concept of PWM is applicable to the arrangement of the rotor magnets. Since the 3rd space harmonic is not presented in three-phase connection of the stator winding, we consider the odd harmonics more than the 3rd one.

2.1 Dimension of Sub-magnet

Figure 1 shows the arrangements of rotor magnets, and Eq. (1) the expressions of the air-gap flux densities produced by them. By adopting the sub-magnet scheme based on the concept of PWM [1], we can eliminate the same number of space harmonics with the sub-ones. For example, the 5th space harmonic can be eliminated by using 80 percent of magnet per pole.

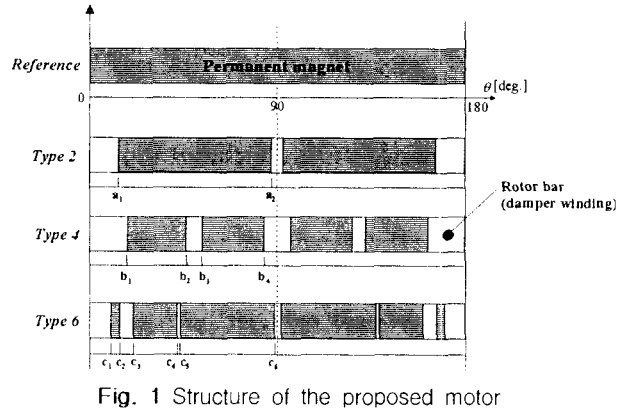

Fig. 1 Structure of the proposed motor

$$B_{r2}=\frac{4B_m}{\pi}\left(\frac{\cos na_1-\cos na_2}{n}\right)\sin nx$$
$$B_{r4}=\frac{4B_m}{\pi}\left(\frac{\cos nb_1-\cos nb_2+\cos nb_3-\cos nb_4}{n}\right)\sin nx \quad (1)$$
$$B_{r6}=\frac{4B_m}{\pi}\left(\frac{\cos nc_1-\cos nc_2+\cos nc_3-\cos nc_4+\cos nc_5-\cos nc_6}{n}\right)\sin nx$$

In the figure, *Type 2* is useful for eliminating two kinds of space harmonics (e.g., 5th, 7th), *Type 4* for four kinds of ones (e.g., 5th, 7th, 11th, 13th), and *Type 6* for six kinds of ones (e.g., 5th, 7th, 11th, 13th, 17th, 19th). In Eq. (1), the angular parameters a, b, and c are related to the dimensions of the sub-magnets in each type and n means the number of higher space harmonics to be eliminated.

2.2 Experimental Machine

The angular parameters of each type can be determined by solving the simultaneous equations in Eq. (1). For example, the parameters a_1 and a_2 in *Type 2* are obtained by putting $B_{r2}=0$ (n=5, 7) in the equation. With the same method, the parameters $b_1 \sim b_4$ in *Type 4* and $c_1 \sim c_6$ in *Type 6* are calculated [2]. Table 1 shows the comparison of each type, and Fig. 2 the configuration of the experimental machine with two main-poles.

In Fig. 2, the thickness of stator core is 36.5[mm], and the stator winding with star connection is 64 turns per slot. In the table, while the sub-magnet scheme causes the reduction of fundamental in air-gap field and the increase of cost, the former reduction can be supplemented by adopting the higher grade of magnet and latter cost becomes cheaper by mass production. Although *Type 6* is most superior in the percentage of space harmonics, its manufacture is difficult. Therefore, we discuss the performance of *Types 2* and *4* hereafter.

3. Hybrid FE-BE Method

The finite element method (FEM) is suitable for analyzing the complicated region including teeth, slots, and magnets, whereas the boundary element method (BEM) for analyzing electromagnetic quantities caused by rotation without remeshing as in the FEM [3, 4]. To investigate the performance of the proposed motor, we adopt the 2-D hybrid FE-BE method.

Figures 3 and 4 show the analysis model and its element division, which the problem domain is classified into two regions. The formulations for FEM, BEM, and the interface condition can be expressed as following Eqs. (2), (3), and (4), respectively.

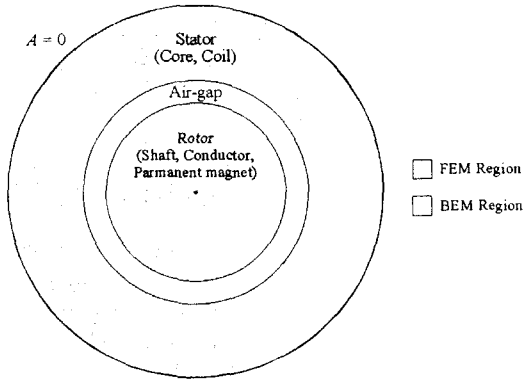

Fig. 3 Analysis model

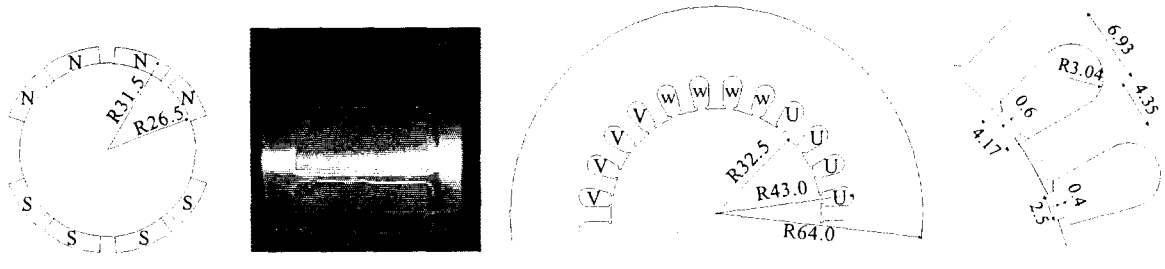

(a) Rotor construction (*Type 4*) (b) Stator (teeth and slots)

Fig. 2 Configuration of proposed motor (Unit: [mm])

Table 1 Comparison of proposed types

Type	Harmonic elimination	Angular parameter [deg.]	Magnet [%]	Harmonics / fundamental [%]						
				1	5	7	11	13	17	19
Reference			100	100	20.00	14.29	9.09	7.69	5.88	5.26
2	5th, 7th,	a_1=15.429, a_2=87.429	80	100	0.00	0.00	5.05	12.45	5.28	6.56
4	5th, 7th, 11th, 13th	b_1=19.103, b_2=46.536 b_3=52.581, b_4=85.451	67	100	0.00	0.00	0.00	0.00	11.06	20.88
6	5th, 7th, 11th, 13th, 17th, 19th	c_1=10.073, c_2=14.307 c_3=20.655, c_4=41.797 c_5=42.817, c_6=88.407	79	100	0.00	0.00	0.00	0.00	0.00	0.00

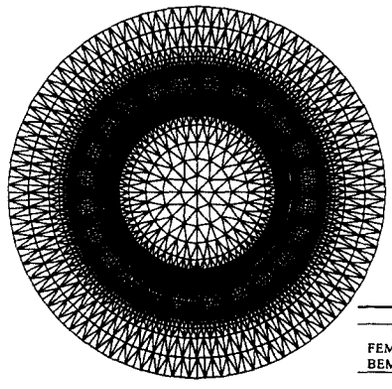

Item	Number
Node	3581
FEM Element	6776
BEM Element	240

Fig. 4 Division of element

$$\nu\left(\frac{\partial^2 A}{\partial x^2}+\frac{\partial^2 A}{\partial y^2}\right)=-J_0+\sigma\left(\frac{\partial A}{\partial t}+\frac{\partial \phi}{\partial t}\right)+\nu_0\left(\frac{\partial M_y}{\partial x}-\frac{\partial M_x}{\partial y}\right) \quad (2)$$

$$C_p A_p=\int_\Gamma \frac{\partial A}{\partial n}\ln\frac{1}{r}d\Gamma-\int_\Gamma \frac{\partial}{\partial n}\left(\ln\frac{1}{r}\right)A d\Gamma \quad (3)$$

$$A_{FEM}=A_{BEM},\quad \frac{\partial A_{FEM}}{\partial n}=-\frac{\mu_{FEM}}{\mu_{BEM}}\frac{\partial A_{BEM}}{\partial n} \quad (4)$$

where A, J_0, ϕ, M, and μ mean the magnetic vector potential, the input current density, the electric scalar potential, the magnetization, and the magnetic permeability, respectively. In addition, we couple both electric circuit and motion equation as shown in Eqs. (5) and (6) with the above hybrid method [5].

$$\begin{cases} E_U+R_U I_U+L_U\dfrac{\partial I_U}{\partial t}-E_V-R_V I_V-L_V\dfrac{\partial I_V}{\partial t}=V_{UV} \\ E_V+R_V I_V+L_V\dfrac{\partial I_V}{\partial t}-E_W-R_W I_W-L_W\dfrac{\partial I_W}{\partial t}=V_{VW} \\ E_W+R_W I_W+L_W\dfrac{\partial I_W}{\partial t}-E_U-R_U I_U-L_U\dfrac{\partial I_U}{\partial t}=V_{WU} \end{cases} \quad (5)$$

$$T_m=J\frac{d^2\theta}{dt^2}\pm T_l \quad (6)$$

where E denotes the electromotive force, L the leakage inductance, T the torque, J the inertial moment, and θ the rotor angle.

4. Analytical & Experimental Results

4.1 Static Characteristics

To grasp the basic behavior of the proposed motors, we begin with the static characteristics. Figure 5 shows the distribution of magnetic flux density in air-gap, Fig. 6 the comparison of cogging-torque, and Fig. 7 the torque versus power angle in an instantaneous value (i.e., I_u= 2[A], I_w=-1[A], I_v=-1[A]) of the three-phase excitation.

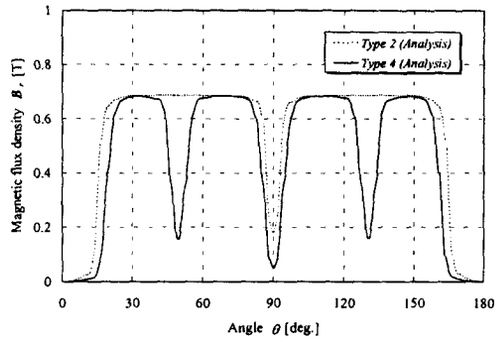

Fig. 5 Air-gap flux distribution

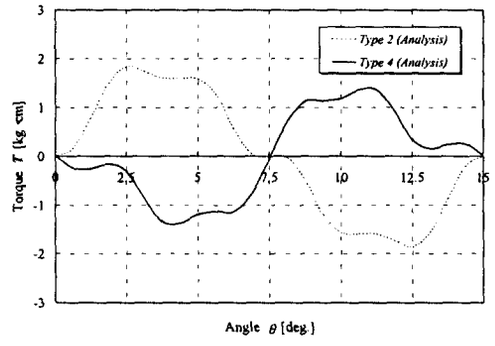

Fig. 6 Comparison of cogging-torque

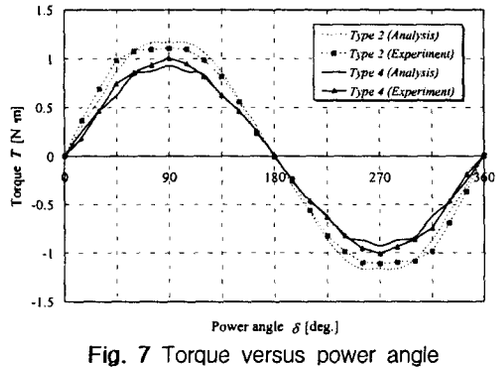

Fig. 7 Torque versus power angle

In the figures, the performances of *Type 4* is inferior to that of *Type 2* because of the less amount of whole magnets, the reduction of magnet can be supplemented by adopting the higher grade ones.

4.2 Synchronous Characteristics

The synchronous behavior of the proposed motor in the steady-state period can be obtained by analyzing the reciprocal action between rotor magnet and stator winding. Figure 8 shows the lines of equipotential at 600[rpm], Fig. 9 the distribution of magnetic flux density, Fig. 10 the torque versus rotational speed at 50[V], and Fig. 11 the torque versus input voltage at 20[Hz].

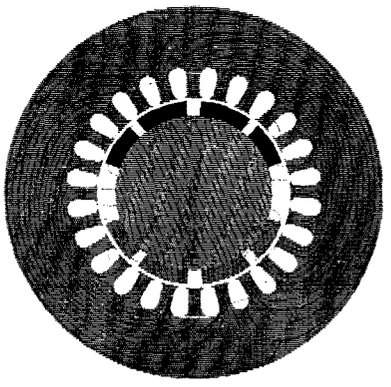

Fig. 8 Equipotentials (600[rpm], $\delta \doteqdot 20.5$[deg.])

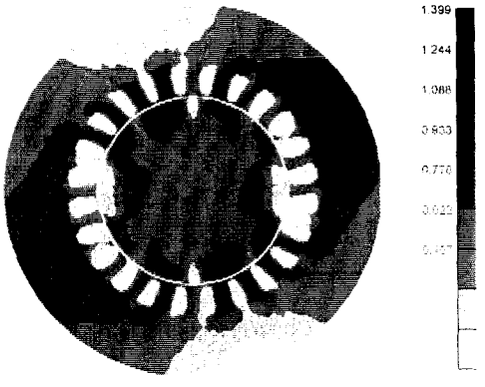

Fig. 9 Magnetic flux (600[rpm], $\delta \doteqdot 20.5$[deg.])

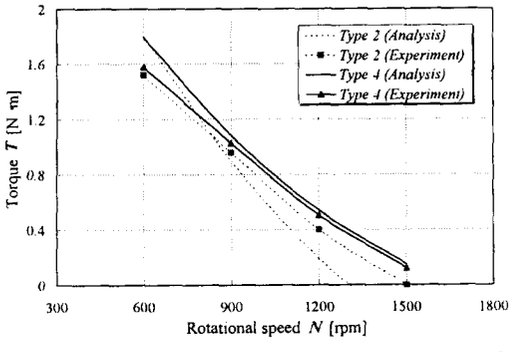

Fig. 10 Torque versus rotational speed (V=50[V])

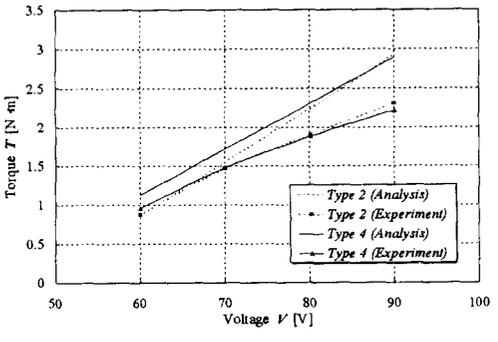

Fig. 11 Torque versus voltage (f=20[Hz])

In Figs. 10 and 11, while the torque of *Type 2* is inferior to that of *Type 4* in the low voltage region (e.g., 50[Hz]) because of its higher induced electromotive force, the former torque becomes to exceed the latter one in the high voltage region (e.g., over than 90[Hz]). In the figures, the reason of error between analytical and experimental results is by the analytical dimension and the error of measurement.

4.3 Transient Characteristics

Since the PMSM has not the field winding, the starting behavior and the reduction of hunting oscillations generally depend on the damper winding (e.g., rotor bar) assuming it is directly line connected. As for the former behavior, we investigate the motor characteristics in the transient period between starting and synchronous speed by both analysis and experiment. Figure 12 shows the rotational speed versus time in the synchronizing process by ramp input of frequency (i.e., 3.33 [Hz/s]) and Fig. 13 by a constant frequency supply (i.e., f=10[Hz], V=120[V]).

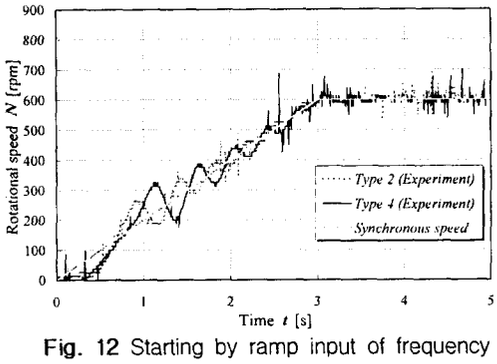

Fig. 12 Starting by ramp input of frequency

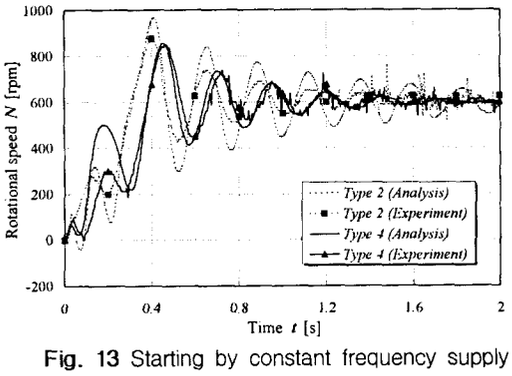

Fig. 13 Starting by constant frequency supply

In Fig. 12, we can recognize that the starting method by ramp input of frequency is not suitable for quick acceleration, because the time period to synchronous speed is indispensable for starting. From the result by constant frequency supply in Fig. 13, we can recognize that the synchronizing process is influenced by the initial position between the rotational magnetic field of stator and the

static field of rotor magnet. The results indicate the synchronizing process by constant frequency supply is underdamped, which always pull into synchronism from higher speed than synchronous one [5].

Figure 14 shows the damping-torque versus slip near the synchronous speed by the constant frequency supply (i.e., f=10[Hz], V=120[V]) and Fig. 15 the configuration of eddy currents developed in rotor bar at 605[rpm]. In Fig. 14, since the torque is much influenced by the whole amount of rotor bar, we can confirm the higher damping torque in *Type 4*.

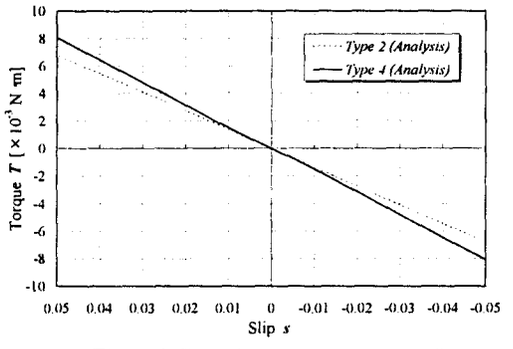

Fig. 14 Damping-torque versus slip

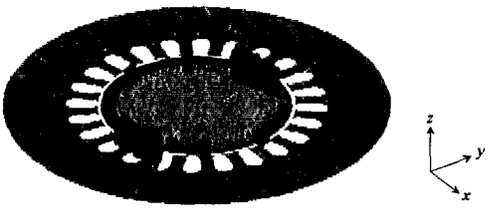

Fig. 15 Configuration of eddy currents at 605[rpm]

4.4 A Novel Starting Method

While the most PMSM is started by the above two methods, we propose a novel starting method in view of ease and efficiency for synchronism. The method is that the higher frequency than synchronizing one is supplied to the starting operation. The high frequency is effective for induction phenomenon in the rotor bar. Figure 16 shows the rotational speed versus time by applying the several high frequencies to the transient period between starting and steady state, which is fixed on 1.255 second.

In the figure, the results indicates that *Type 4* is superior to *Type 2* in both the acceleration at starting and the convergence of hunting oscillation. In Figs. 16 (a) and (b), while the synchronizing process are under- and over-damped respectively, the process becomes smooth by supplying the appropriate frequency at starting period as shown in Fig. 16 (c). From the figures, we can also recognize that the underdamped synchronism is more stable than overdamped one [6]. Figure 16 (d) shows a failed example in the synchronizing process of *Type 2* because of its less torque and speed.

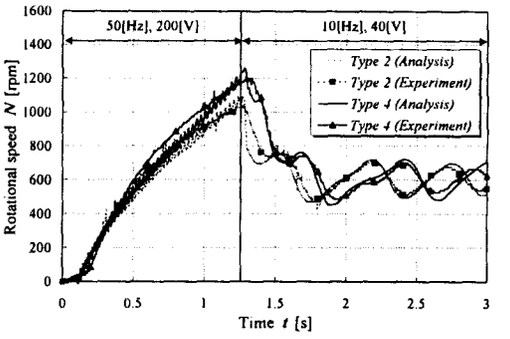

(a) f=50[Hz], V=200[V]

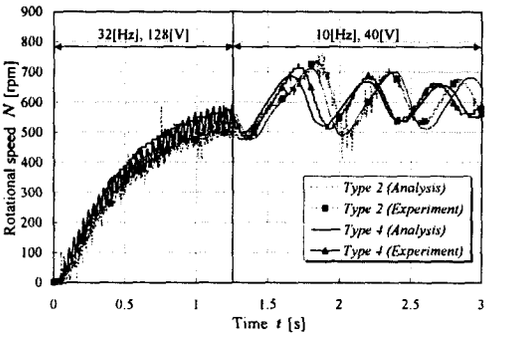

(b) f=32[Hz], V=128[V]

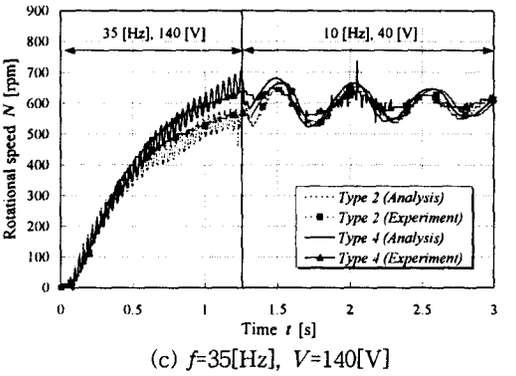

(c) f=35[Hz], V=140[V]

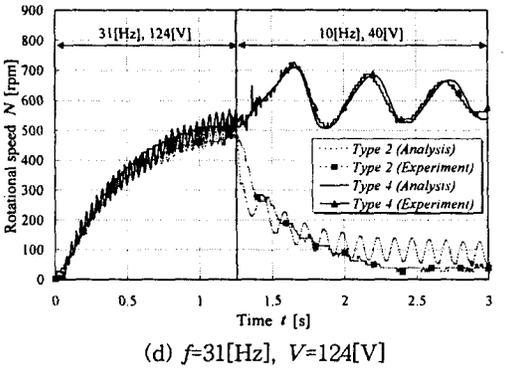

(d) f=31[Hz], V=124[V]

Fig. 16 Starting by two stages of frequencies

5. Conclusion

The purpose of this paper is to derive an optimal rotor construction in the permanent magnet synchronous motor (PMSM) for electric vehicle (EV). By applying sub-magnet scheme based on the concepts of pulse width modulation (PWM) to the rotor construction, we can achieve both the reduction of higher space harmonics and the enhancement of damping effects. For investigating the dynamic and transient characteristics of the motor, we adopt 2-D hybrid FE-BE method coupled with both electric circuit and motion equation.

By the analytical and experimental results, we recognize the followings :

1) The more number of sub-magnets produces the less space harmonics and the higher damping effects.
2) The analysis precision is improved by coupling the hybrid FE-BE method with both electric circuit and motion equation.
3) The rotor bars between neighboring sub-magnets contribute to the self-starting of rotor. In addition, the starting method by two stages of supply frequencies is effective for the self-starting.

From the viewpoint of the above advantages, we conclude that *Type 4* is effective for practical use and confirm the confidence of our analysis method.

References

[1] B.D. Bedford and R.G. Hoft, "Principles of inverter circuit", John Wiley & Sons. Inc., pp. 254-261, 1964.

[2] T. Onuki, et al., "Optimal Rotor Construction of Synchronous Motor with Plural Permanent Magnets per Pole", IEE-EMD'97, CP-No. 444, pp. 31-35, 1997.

[3] T. Onuki, et al., "Hybrid FE and BE method applied to nonlinear magnetic field analysis", IEEE Trans. on Magnetics, Vol. 30, No. 5, pp. 2908-2911, 1994.

[4] W.J. Jeon, "Development of the Linear Motor for Special Purpose & Improvement of the Performance", Waseda Univ. Diploma No. 2601, Japanese Ministry of Education No. 1259, pp. 143-145, 1998.

[5] K. Kurihara, et al., "Transient Performance Analysis of Permanent Magnet Synchronous Motors Using the Finite Element Analysis", Trans. of IEE Japan, Vol. 114-D, No. 5, pp. 551-560, 1994.

[6] T. Onuki, et al., "An Approach to Enhance the Performance of Linear Synchronous Motor with Induction Starting", Int. Conf. on Electrical Machines (ICEM'98), Vol. 2, pp. 1083-1088, 1998.

[7] JR Hadji-Minaglou and G. Henneberger, "Comparison of different motor types for electric vehicle application", EPE Journal, Vol. 8, No. 3-4, pp. 46-55, September 1999.

저 자 소 개

전 우 진 (田 宇 鎭)

1967년 3월 3일 생. 1991년 2월 건국대 전기공학과 졸업. 1995년 3월 와세다대학 전기공학과 대학원 석사과정, 1998년 3월 박사과정 졸업 (공박). 1995~1998년 日本文部省 국비장학생. 현재, 동 대학 교원 (전임), 日本電氣學會 리니어 해석 및 설계위원회 간사보좌, 日本航路標識協會 자연에너지응용 조사위원회 작업부 위원장, (주) 동원론 기술담당. 관심분야: 전자장수치해석, 리니어모터, 전기자동차, 고속전철, 유도가열 등

Tel : +81-3-5286-3219, E-mail : wjeon@ieee.org

Hideki Watanabe (渡辺 英樹)

1974년 10월 4일 생. 1997년 3월 와세다대학 이공학부 전기공학과 졸업. 1999년 3월 동 대학원 석사과정 졸업. 1999년 4월 (주) SONY 입사. 현재는 (주) SONY HNC HDC ATV Div. Co. DT상품설계부 설계1과 근무

Yushi Kamiya (紙屋 雄史)

1969년 8월 20일 생. 1993년 3월 와세다대학 이공학부 전기공학과 졸업. 1995년 3월 동 대학원 석사과정, 1997년 3월 박사과정 졸업 (공박). 동 대학 교원 (전임) 및 日本運輸省 운수기술연구원 역임. 현재, 日本國立群馬大學 대학원 교육학연구과 조교수, 와세다대학 이공학총합연구센터 객원연구원

Takashi Onuki (小貫 天)

1929년 7월 31일 생. 1951년 3월 와세다대학 전기공학과 졸업. 1951년 4월 日本通産省 공업기술원 전기시험소 입소. 1954년부터 와세다대학 근무 (공박). 1988년~1992년 동 대학 이공학총합연구센터 소장. 日本電氣學會 靜止器, 回轉機, 리니어위원회 위원장 역임. 동 학회 논문상, 업적상 수상. IEEE Fellow

전 혜 정 (田 惠 晶)

1968년 4월 8일 생. 1991년 2월 이화여대 전산학과 졸업. 1993년 2월 동 대학원 석사과정 졸업. 현재, LG종합기술원 선임연구원, 한국과학기술원(KAIST) 대학원 전산학과 박사과정. 주관심분야는 컴퓨터구조론 및 수치계산용 프로그램의 개발.

Tel : 02-526-4126, E-mail : hjeong@lgcit.com